An Optimized Distributed Cooperative Control to Improve the Charging Performance of Battery Energy Storage in a Multiphotovoltaic Islanded DC Microgrid

Poursafar, Noushin; Taghizadeh, Seyedfoad; Hossain, M. J.; Guerrero, Josep M.

Published in:
IEEE Systems Journal

DOI (link to publication from Publisher):
10.1109/JSYST.2021.3070883

Publication date:
2022

Document Version
Accepted author manuscript, peer reviewed version

An Optimized Distributed Cooperative Control to Improve the Charging Performance of Battery Energy Storage in a Multiphotovoltaic Islanded DC Microgrid

Noushin Poursafar, *Student Member, IEEE*, Seyedfoad Taghizadeh, *Student Member, IEEE*, M. J. Hossain, *Senior Member, IEEE*, and Josep M. Guerrero, *Fellow, IEEE*

***Abstract*—When multi-photovoltaic (PV) energy sources are installed in dc microgrids (DCMGs), an optimized distributed controller is essential to provide efficient, economical, and reliable operation. This article proposes an optimized distributed cooperative control method for multi-PV energy sources in an islanded DCMG. Unlike conventional control methods for DCMGs, the proposed distributed cooperative control method is capable of obtaining a constant total generated power from PVs, thus minimizing the impact of the intermittent nature of PVs on the total generation. This operation subsequently reduces the charging stress on the backup energy storage system (BESS) and increases the lifetime of the BESS in the DCMG. The proposed control method can also intelligently reduce the total generation cost of the DCMG via monitoring and analyzing the information of energy sources and minimizing the quadratic cost function. The dynamic model of the proposed controller is thoroughly analyzed, and its effectiveness in terms of providing controllable generated power and cost reduction is validated for different generation-demand scenarios.**

***Index Terms*—Cooperative control, dc microgrid (DCMG), distributed control, power flow control, voltage stability.**

I. Introduction

TOGETHER with the increasing number of dc-based distributed generators (DGs), interest in the installation of dc microgrids (DCMGs) has been increasing due to their ability to reduce the costs and energy dissipation associated with dc/ac conversion. Unlike ac microgrids (ACMGs), the overall stability of DCMG systems depends upon voltage regulation since there is no need for reactive power interaction.

In DCMGs, the intermittent nature of renewable sources causes their output power to fluctuate and disturbs the voltage stability of the dc bus. To address this issue, various strategies have been proposed in the literature that focus on either connecting the DCMG to the main grid (grid-connected mode) or using backup energy storage systems (BESS) in grid-isolated (islanded) DCMGs. In a grid-connected DCMG, the mismatch between generation and loads' demand is controlled via transferring power from/to the main grid [1]–[3]. On the other hand, using BESS assistance, the mismatch between generation and demand is controlled via charging or discharging the BESS [4]–[7].

Although better stability of the dc-bus voltage can be achieved in grid-connected DCMGs due to the existence of a main grid, this can be challenging in remote and rural areas where either the grid connection is not available or the grid is weak and cannot robustly regulate the bus voltage of the DCMG. As a result, BESS assistance is required as a reliable solution for grid-connected DCMGs and especially for islanded DCMGs. However, a well-designed power management system is required for islanded DCMGs; this system is the main focus of this article.

Various power management systems have been proposed in the literature for islanded DCMGs. In [8]–[10], the authors propose a distributed coordination method to manage power among multi-islanded DCMGs. The distributed control method provides a balance between the total generation and the load demand by regulating the common dc bus voltage. To do so, the voltages of all the connected DCMGs are measured and converged to an average voltage by using the distributed control method. While this method ensures the regulation of the common dc bus voltage, it does not maintain the voltage of each connected DCMG at a constant value. To control the bus voltage of a single DCMG without connecting to other DCMGs, a switching control method is used in [11] to coordinate the operation of integrated DGs, including a PV, a wind turbine, a micro-turbine (MT), and a BESS. This technique monitors and collects information on weather conditions and load demand. Then, based on the collected data, it makes a decision on whether to connect or disconnect the MT and/or the BESS to maintain a balance between demand and generation. Although this method ensures the stability of the dc-bus voltage, it has the drawbacks of high complexity and cost because of its use of more resources (PVs, MTs, DGs, and BESS) and mass data processing, which requires costly processors and control centers. In addition, the switching control strategy suffers from high switching disturbances, which create additional fluctuations on

Manuscript received July 29, 2020; revised February 1, 2021; accepted March 29, 2021. *(Corresponding author: Noushin Poursafar.)*

Noushin Poursafar and Seyedfoad Taghizadeh are with the School of Engineering, Macquarie University, Macquarie Park, NSW 2019, Australia (e-mail: noushin.poursafar@students.mq.edu.au; s.t.taghizadeh@ieee.org).

M. J. Hossain is with the School of Electrical and Data Engineering, University of Technology Sydney, Ultimo, NSW 2007, Australia (e-mail: jahangir.hossain@uts.edu.au).

Josep M. Guerrero is with the Department of Energy Technology, Aalborg University, 9220 Aalborg, Denmark (e-mail: joz@et.aau.dk).

Digital Object Identifier 10.1109/JSYST.2021.3070883

the dc-bus voltage. To solve this issue, [12] and [13] suggest using a continuous voltage controller for the BESS. During an overvoltage event of the dc bus, which results from the loads' demand being lower than the generation, the voltage controller charges the BESS to consume the overgenerated power. On the other hand, during an undervoltage event of the dc bus, the BESS is discharged to cover the power shortage. In [14]–[16], the voltage controller uses a proportional integral (PI) controller for generating the reference signal for the inner current controller. In [17]–[20], the authors suggest using a droop controller instead of a PI controller. In [21] and [22], a nonlinear droop controller and adaptive droop controller are used, respectively, to enhance the effect of the droop control on the dc-bus voltage regulation. In [23] and [24], the authors suggest using a model predictive control approach to control the dc-bus voltage in an islanded DCMG including PVs as sources. According to this method, two operational modes are defined for the switches of the BESS converter. In each mode, the error of the dc-bus voltage is calculated based on comparing the predicted status of the dc-bus voltage in the next sampling time and the current measured status of the dc-bus voltage in the current time. Then, the mode that provides the fewest error will be selected as a command for the BESS converter. Using a different strategy, the authors in [25]–[27] use a power control method instead of a voltage control method to charge and discharge the BESS. According to this method, if the total generation is more than the load demand, the BESS draws the excess power from the bus during charging. On the other hand, when the total generation is less than the load demand, the BESS injects the power required to maintain a balance between the generation and the load demand. In all the above-mentioned methods, a BESS is solely responsible for regulating the dc-bus voltage, which is effective during normal operation of the DCMG. However, during a sharp change of power (i.e., caused by a failure of a PV source), the capacity of the BESS might not be sufficient to regulate the dc-bus voltage. To avoid this limitation, the authors in [28]–[31] suggest using additional storage systems, such as supercapacitors and flywheels to assist the BESS in regulating the dc-bus voltage. However, such additional equipment inevitably increases the cost and bulkiness of the system.

The main drawback of all these conventional methods is the high dependency of charging/discharging of the BESS (or the other energy storage systems) on the intermittent nature of renewable energy sources. This is because any variation in solar irradiation or wind speed changes the output power of the renewable energy generators, and, consequently, the BESS needs to be charged/discharged with the same fluctuating ratio to keep the dc-bus voltage stable. This ratio is significantly higher during a critical situation when an unexpected failure occurs in one or more renewable energy generators, causing a sudden drop in generation and a subsequent voltage drop at the dc bus. In both normal and critical situations, the high charging/discharging ratio of the BESS increases the stress on the battery, which can adversely affect its lifetime. Moreover, during a critical situation (i.e., renewable source failure) when the BESS requires an immediate discharging operation, such an inevitable discharging of the BESS undesirably consumes the stored energy of the battery so that during the absence of sunlight, when the PVs are in standby mode, the BESS is not capable of supplying enough energy for the local loads. Finally, the conventional methods only focus on maintaining the stability of DCMGs without paying attention to the cost of generation. This matter requires close attention, as large-scale DCMGs will be deployed and installed in the future.

To solve the above-mentioned problems, this article presents a distributed coordinating control strategy for dc–dc converters that connect photovoltaic (PV) energy sources to a DCMG. Using the proposed control strategy, a constant power is supplied for both local loads and the BESS, which significantly decreases the charging/discharging fluctuations of the BESS. In addition, the proposed distributed coordinating control method intelligently manages the power distribution in the DCMG with the aim of saving more energy stored in the BESS during a normal operational mode and a source failure. The proposed method also minimizes the cost of purchasing power from neighbors. In the proposed method, the primary conventional control used for dc–dc converters is improved by having three parallel controllers: a dc-bus voltage controller to regulate dc-bus voltage, a power controller that regulates the total generated power of all PVs to a constant or adjustable value, and an energy cost minimization controller (optimizer) that uses neighbors' data through a distributed framework to reduce the total generation cost of the DCMG. During the operation, the dominant voltage controller maintains the stability of the dc-bus voltage, while the power controller and the optimizer generate correction terms for the current controller. The proposed system has the following contributions compared to the above-mentioned conventional methods.

1) Minimize the impact of the intermittent nature of PVs on the total generation, thus obtaining constant power from renewable energy sources.
2) Improve charging/discharging ratio of the BESS that extends the availability of the BESS in the DCMG. This ensures sufficient state-of-charge (SOC) and reduces the charging stress on the battery, which, as a consequence, can increase the battery lifetime.
3) Integrate an optimizer with the distributed controller to reduce the total generation cost of the DCMG using the neighbor's generation information.

The rest of the article is outlined as follows. The proposed control strategy is presented in Section II. In Section III, the dynamic model of the proposed controller is explained in detail. The design procedure is described in Section IV. Section V presents the results and discussion, and Section VI provides the conclusion.

II. Proposed Control Strategy for DCMG

The overall configuration of the DCMG is shown in Fig. 1. This model includes a local grid that consists of a 8-kW PV, PV_5 operating in maximum power point tracking (MPPT) mode, dc loads with load variation between 5 and 12 kW, and a BESS. There are also four 12-kW PVs in the neighborhood, PV_1–PV_4, which are controlled by the proposed coordinating control method to assist PV_5 to supply a constant power for the local loads and the BESS as shown in Fig. 2. The lithium-ion based 350-V BESS unit, which is connected to the dc-bus via a bidirectional converter, is responsible for maintaining a balance between the supplied power and the load demand via its charging/discharging operation. It absorbs power when the supplied power is more than the load demand and injects power when the supplied power is less than the load demand.

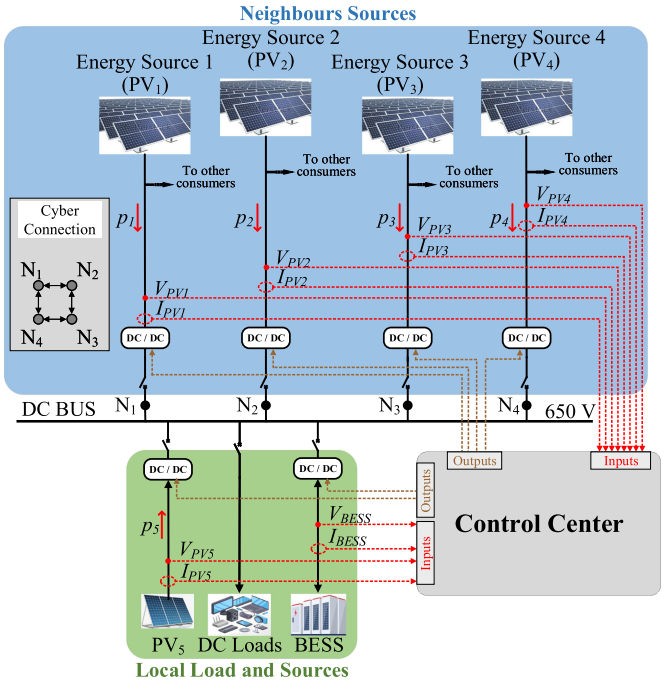

Fig. 1. Configuration of the DCMG.

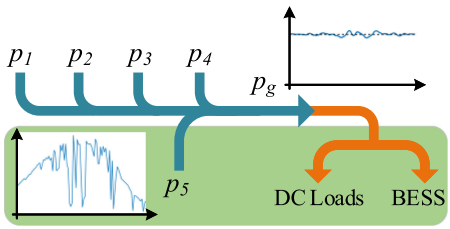

Fig. 2. Diagram of power distribution in the DCMG.

SunPower 315 NE series solar panels in five strings of six panels are used to model the PV_5 system, and the same model of solar panels in two strings of 20 panels is used to model the PV_1–PV_4 systems. The solar irradiation shown in Fig. 3(a) is used for PV_5. As shown, the maximum irradiation occurs during midday with 1000 W/m^2, and its minimum value of 200 W/m^2 is recorded during sunrise, sunset, and cloud shading. To decrease the simulation time, the daytime (6 A.M.–8 P.M.) is downscaled to a 3.5-s duration (from $t = 0$ s to $t = 3.5$ s). To differentiate between the input irradiation of the PVs, the irradiation pattern of Fig. 3(a) is shifted by +1, +0.5, –1, and –0.5 s and applied to PV_1–PV_4, respectively. In this article, a constant temperature $T = 25°$C is used for all PVs. This is because the effect of daytime temperature variation, which is approximately 20°C, on the output power of a PV is significantly less than the effect of the solar irradiation fluctuations [Fig. 3(b) and (c)] [32]. As shown in Fig. 3(b), the maximum power (MP) of a PV significantly changes from 0.2 to 1 p.u. when the solar irradiation changes from 200 to 1000 W/m^2, while the temperature is fixed at $T = 25°$C. On the other hand, if the temperature changes from 15 to 35°C, the MP of a PV slightly changes from 1.03 to 0.97 p.u., while the solar irradiation is fixed at $Ir = 1000$ W/m^2. As a result, a constant temperature ($T = 25°$C) is used for the analysis throughout the article. The system parameters of the DCMG model are summarized in Table I.

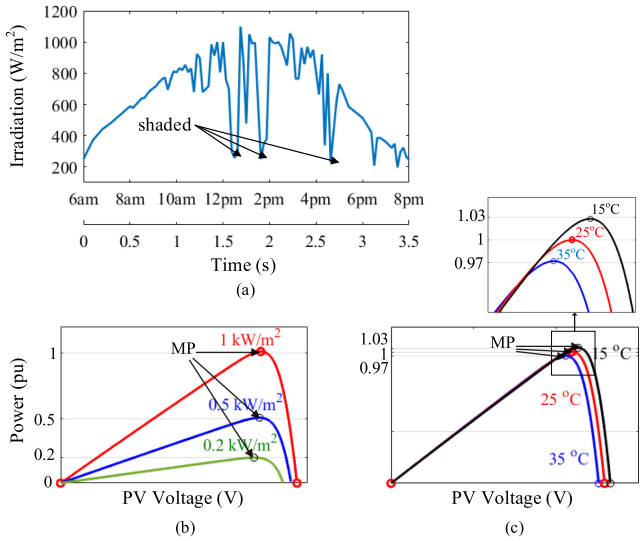

Fig. 3. Solar irradiation.

TABLE I
SYSTEM PARAMETERS

Circuit Parameter	Item	Value
L_p	boost converter inductance	5 mH
L_b	bidirectional converter inductance	5 mH
C	dc-bus capacitor	1 mF
f_{sw}	switching frequency of all PWMs	20 kHz
t_{sm}	simulation sampling time	1 μs

A. Optimization and Cost Minimization

In a DCMG, cost can play an important role when there is a mismatch between the local generation (PV_5) and local load demands. In this case, the purchasing power from neighboring local generators is required, and identifying the agent that offers the lowest cost to dispatch the energy is preferred. Mathematically speaking, the economic dispatch problem is to minimize the total cost $C(\mathbf{p})$ for supplying the power shortage between demanded power and local generation

$$\text{minimize} C(\mathbf{p}) = \sum_{i=1}^{4} C_i(p_i)$$

$$\text{subject to} \sum_{i=1}^{4} p_i + p_5 = P_g^* \tag{1}$$

where p_i and $C_i(p_i)$ are the transferred power and the cost function of PV_i, respectively, p_5 is the MP of PV_5 and P_g^* is the desired total generated power from all PVs. In this article, P_g^* is constant and set by an operator to get a constant power from variable-output power sources. The details of setting P_g^* are explained in Section II-D. As equation (1) shows, the desired generation P_g^* is equal to the sum of the MP of the local source (PV_5) and the power transferred from the neighbor sources with minimum cost. On the other hand, P_g^* is equal to the sum of the dc-load demand $P_{\text{dc-load}}$ and the BESS power P_{BESS} to maintain a balance in power between the total generation and the consumed power in the DCMG

$$P_g^* = P_{\text{dc-load}} + P_{\text{BESS}}. \tag{2}$$

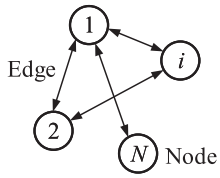

Fig. 4. Communication graph.

The economic dispatch problem (1) can be formulized as a Lagrange function with Lagrange multiplier λ that needs to be minimized

$$L(\mathbf{p},\lambda) = C(\mathbf{p}) + \lambda\left(P_g^* - p_5 - \sum_{i=1}^{4} p_i\right). \tag{3}$$

The solution of the Lagrange function is a stationary point where the partial derivation of L is zero with respect to all variables [33]

$$\begin{cases} \frac{\partial L}{\partial p_i} = 0 \Rightarrow \frac{dC_i}{dp_i} = \lambda \\ \frac{\partial L}{\partial \lambda} = 0 \Rightarrow \sum_{i=1}^{4} p_i = P_g^* - p_5. \end{cases} \tag{4}$$

Equation (4) shows that the problem (1) is minimized if the incremental costs of all energy sources reach a consensus value.

Since the output power of PVs is controllable, they can be considered as dispatchable sources, and the quadratic cost function presented in [34] and [35] can be used in the cost minimization problem (1)

$$C_i(p_i) = \alpha_i + \beta_i p_i + \gamma_i p_i^2 \tag{5}$$

where $\alpha_i, \beta_i, \gamma_i$ are coefficients of the cost function of source i and indicate operating costs and converter loss-efficiency. Therefore, with definition λ_i as the incremental cost of source i

$$\lambda_i = \frac{dC_i}{dp_i} = \beta_i + 2\gamma_i p_i \tag{6}$$

(4) can be written as

$$\lambda_i = \lambda^* \ \forall i \tag{7}$$

where λ^* is the consensus value of all energy sources.

The graph theory and consensus algorithm, which are explained in the following sections, are used to achieve a unique consensus value for the incremental cost of energy sources.

B. Graph Theory

Let us consider a communication network with a set of nodes $\mathbf{V} = \{v_1, v_2, \ldots, v_N\}$ connected through a set of edges $\mathbf{E} = \mathbf{V} \times \mathbf{V}$ that represent control agents and communication links (Fig. 4). A graph with N nodes can be represented by an adjacency matrix $\mathbf{A} = [a_{ij}] \in \mathbb{R}^{N\times N}$ that is associated with the graph edges, where a_{ij} is the weight for information exchanged between agents i and j. $a_{ij} = 0$ denotes the fact that node i cannot receive information from node j. In this graph, the set of neighbors of node i is denoted by N_i.

An important matrix in graph theory is the diagonal in-degree matrix $\mathbf{D}_{in} = [d_{ij}]$ where d_{ii} is the row-sum of the ith row of the adjacency matrix $d_{ii} = \sum_{i=1}^{n} a_{ij}$. Therefore, the Laplacian matrix can be defined as $\mathbf{L} = \mathbf{D}_{in} - \mathbf{A}$, which has a zero eigenvalue with the corresponding eigenvector $\mathbf{v} = [1 \ldots 1]^T$.

A graph is said to have a spanning tree if it contains a root node, from which there exists at least one direct path to every other node. If a graph has a spanning tree, rank$(\mathbf{L}) = N - 1$, and the only solution to $\mathbf{Lx} = 0$ is $\mathbf{x} = c[1 \ldots 1]^T$ where c is a constant.

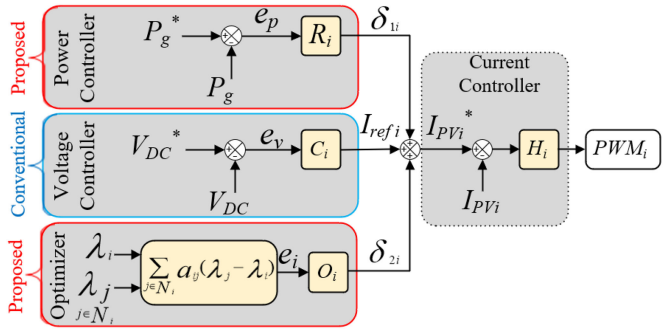

Fig. 5. Proposed distributed controller.

C. Consensus Algorithm

Consider a network of agents with dynamics $\dot{x} = u$ that are in communication with their neighbors to reach an agreement. According to [36], the linear system

$$\dot{x_i}(t) = \sum_{j \in N_i} a_{ij}(x_j(t) - x_i(t)) \tag{8}$$

is a distributed consensus algorithm that guarantees convergence to a consensus value via local interactions. The dynamics of the group of agents can be written as

$$\dot{\mathbf{x}} = -\mathbf{Lx} \tag{9}$$

where $\mathbf{L}$ is the Laplacian matrix of the agent network graph. If the agents' graph has a spanning tree, then the consensus value or the system steady-state value is unique and is equal to the average of the initial states of all nodes $\frac{1}{n}\sum_{i=1}^{n} x_i(0)$.

D. Proposed Distributed Cooperative Control

Fig. 5 shows the distributed cooperative control method proposed in this article. Unlike the conventional methods that use only an outer voltage controller and an inner current controller, [13], the method proposed in this article, employs two additional regulators, a power controller, and a cost optimizer, in parallel with the outer voltage controller to enhance the performance of the distributed control system. As shown in Fig. 5, similar to the conventional approach, the voltage controller compares the dc-bus voltage V_{DC} with its reference value V_{DC}^* and generates a reference I_{ref_i} for the current controller through a PI controller C_i. Then, the current controller adjusts the duty cycle of the converter based on generated I_{ref_i}. The proposed power controller and a cost optimizer generate two correction terms: δ_{1i} and δ_{2i}. These correction terms are added to I_{ref_i} to regulate the total generated power and minimize the cost function of (1), respectively. As shown in Fig. 5, the power controller compares P_g, which is the total generation of the local source and the power received from the neighbor

TABLE II
CONTROL PARAMETERS

Control Parameter	Item
K_{PH} , K_{IH}	proportional and integral gains of H_i
K_{PC} , K_{IC}	proportional and integral gains of C_i
K_{PR} , K_{IR}	proportional and integral gains of R_i
K_{PO} , K_{IO}	proportional and integral gains of O_i

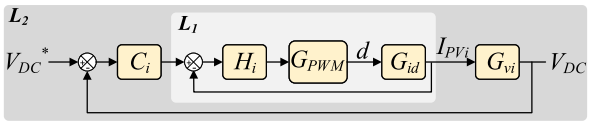

Fig. 6. Voltage control loop.

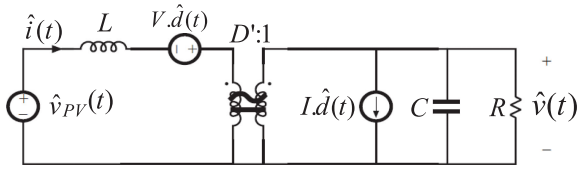

Fig. 7. Circuit equivalent of a dc/dc boost converter.

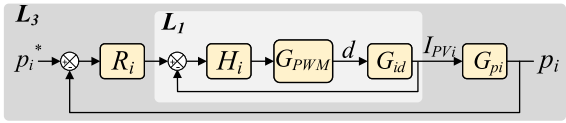

Fig. 8. Power control loop.

($P_g = \sum_{i=1}^{4} p_i + p_5$), with the reference P_g^*. The result is the generation of the correction term δ_{1i} through the PI controller R_i. As already mentioned, P_g^* is supposed to be set externally and can be based on a daily consumption of a local grid. P_g^* is recommended to be set to its allowed maximum, which often happens at midday when the solar source is at its maximum level. As a result of operating the proposed control system, a constant power is always transferred from the PVs to the local loads and the BESS. This can significantly increase the lifetime of the BESS due to the decrease in the charging/discharging ratio of the BESS.

By using the optimizer, nodes N_1–N_4 (as shown in Fig. 1) communicate with each other with the adjacency matrix $\mathbf{A} = [a_{ij}] \in \mathbb{R}^{N\times N}$ and generate an incremental cost error for agent i

$$e_i = \sum_{j \in N_i} a_{ij}(\lambda_j - \lambda_i). \tag{10}$$

This error term is then fed to the PI controller O_i to generate the correction term δ_{2i}. If e_i is negative (positive), the controller decreases (increases) δ_{2i}, which in turn reduces (increases) the setpoint $I^*_{\text{PV}i}$ and the incremental cost of source i. Based on what is explained in Section II-C, all control agents converge to a consensus value, and all error terms become zero at the steady state. The control parameters of the proposed controller are defined in Table II, and the designed values are presented in Section VI-A.

III. DYNAMIC MODEL OF THE DISTRIBUTED COOPERATIVE CONTROLLER

In this section, the dynamic models of the three control loops (voltage control loop, power control loop, and cost control loop) required for the design of the proposed distributed coordinating controller are presented separately.

A. Voltage Control Loop

The voltage control loop as the main control loop is presented in Fig. 6. In this article, G_{PWM} is considered to be unity for simplification. Using the small-signal model presented in [37] for the boost converter (Fig. 7), G_{vd} is given by

$$G_{vd} = \frac{\hat{v}}{\hat{d}} = \frac{V}{D'}\frac{(-Ls + RD'^2)}{(RLCs^2 + Ls + RD'^2)} \tag{11}$$

and G_{vi} is

$$G_{vi} = \frac{\hat{v}}{\hat{i}} = \frac{1}{D'}\frac{-Ls + RD'^2}{RCs + 2}. \tag{12}$$

So, G_{id} is equal to

$$G_{id} = \frac{\hat{i}}{\hat{d}} = \frac{G_{vd}}{G_{vi}} = V\frac{(RCs + 2)}{(RLCs^2 + Ls + RD'^2)} \tag{13}$$

where V, I, and D are the dc quiescent value of the dc-bus voltage, the inductor current, and the duty cycle of the converter, respectively, and $\hat{v}$, $\hat{i}$, and $\hat{d}$ are their small ac variations. $\hat{v}_{\text{PV}}$ is the small ac variation of PV voltage and $D' = 1 - D$.

B. Power Control Loop

In the power control loop, the power error e_p as shown in Fig. 5 is equal to $P_g^* - (\sum_{j=1}^{4} p_j + p_5)$ or $P_g^* - p_5 - \sum_{j\in N_i} p_j - p_i$. One can define

$$p_i^* = P_g^* - p_5 - \sum_{j\in N_i} p_j. \tag{14}$$

Then the power error can be written as $e_p = p_i^* - p_i$. The simplified model of proposed power control loop is shown in Fig. 8. To find G_{pi}, assume that the output voltage, current, and power of a PV are equal to the dc quiescent values plus the superimposed small ac variations: $v_{\text{PV}}(t) = V_{\text{PV}} - \hat{v}_{\text{PV}}(t)$, $i_{\text{PV}}(t) = I_{\text{PV}} - \hat{i}_{\text{PV}}(t)$ and $p_i(t) = P_i - \hat{p}_i(t)$. Substituting $v_{\text{PV}}(t)$ and $i_{\text{PV}}(t)$ into $p_i(t) = v_{\text{PV}}(t) \times i_{\text{PV}}(t)$ results in

$$P_i - \hat{p}_i(t) = V_{\text{PV}}I_{\text{PV}} + \hat{v}_{\text{PV}}(t)\hat{i}_{\text{PV}}(t) + V_{\text{PV}}\hat{i}_{\text{PV}}(t) + \hat{v}_{\text{PV}}(t)I_{\text{PV}}. \tag{15}$$

By neglecting both dc terms, which are equal on both sides of the equations, and the second-order ac terms, which are much smaller than the first-order terms, the small-signal model of the output power can be written as

$$\hat{p}_i(t) = V_{\text{PV}}\hat{i}_{\text{PV}}(t) + \hat{v}_{\text{PV}}(t)I_{\text{PV}}. \tag{16}$$

Since the current perturbation is much larger than that of the voltage, (16) can be written as $\hat{p}_i(t) = V_{\text{PV}}\hat{i}_{\text{PV}}(t)$. Therefore, G_{pi} is

$$G_{pi} = V_{\text{PV}}. \tag{17}$$

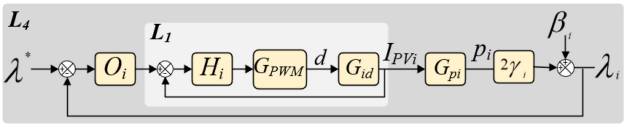

Fig. 9. Cost control loop.

C. Cost Control Loop (Optimizer)

In the cost control loop, the input term (10) can be replaced with (18) without a loss of generality,

$$e_i = (\lambda^* - \lambda_i) \tag{18}$$

where λ^* is the consensus value of all power agents. Using (17), the simplified block diagram of the cost control loop is shown in Fig. 9, and the design procedure is explained in the following section.

IV. Design Procedure

In this section, the dynamic models of Section III are used to design the proposed distributed coordinating controller. Then, the designed parameters are used for performance analysis of the proposed system in different case scenarios, including comparison with the conventional method. The control parameters are designed based on the linear models to achieve the best performance (lowest overshoot/undershoot and settling time) of the system. Although the nonlinearities are neglected and can change the dynamic of the system in real applications, the preformed optimum design minimizes their effect and ensures the stability of the system. To design the control system for the DCMG, the design procedure is divided into three parts: 1) design the proposed controller for dc–dc converters of PV_1 to PV_4; 2) design a controller for the converter of PV_5 to operate in the MPPT mode; and 3) design an inner current controller and an outer voltage controller for the bidirectional converter of the BESS.

A. Design the Proposed Controller for PV_1 to PV_4

To design the proposed distributed coordinating controller, including the inner current controller and the outer controllers (voltage controller, power controller, and optimizer), root locus analysis is used for the dynamic models obtained in Section III, and the following steps are followed.

Step 1: Initially, the inner current control loop (L_1), which is the closest controller to the plant, is designed. Accordingly, the transfer function in (13) is used. While the dc loads are assumed to vary between 35 and 80 Ω (12–5 kW), controllers are designed to keep the system stable within this range. To design the controller H_i in Fig. 5, $K_{\rm PH}/K_{\rm IH}$ is set to 0.005. Then, based on the rlocus plot of the system, $K_{\rm IH}$ is tuned. Fig. 10(a) and (b) shows the rlocus of the system for $R = 35\,\Omega$ and $R = 80\,\Omega$, respectively. In this article, our design criteria are to find the fastest response with the lowest overshoot while keeping the duty cycle less than one ($d < 1$). Root locus plots are used to observe the overshoot and settling time, and to check condition $d < 1$, the following transfer function is used:

$$d = \frac{H_i}{1 + G_{id}H_i} I_{\rm max} \tag{19}$$

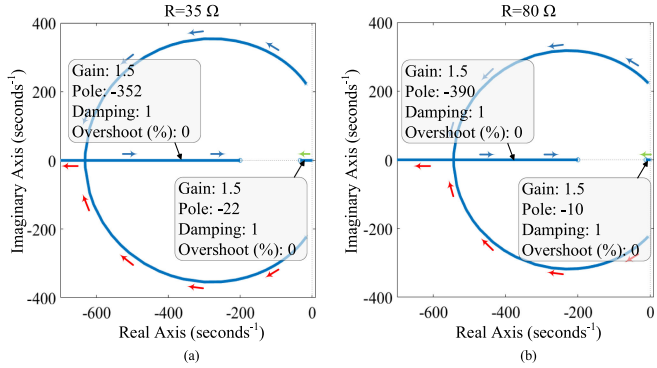

Fig. 10. Current control loop rlocus for (a) $R = 35\,\Omega$ and (b) $R = 80\,\Omega$.

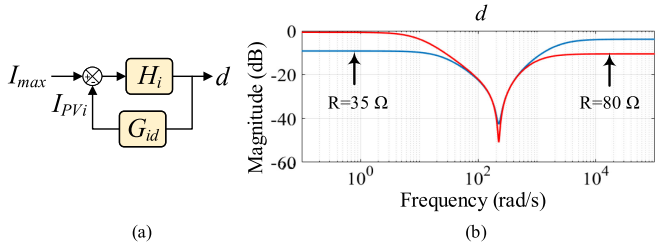

Fig. 11. PWM duty cycle of the boost converter based on the maximum current transferred from a PV.

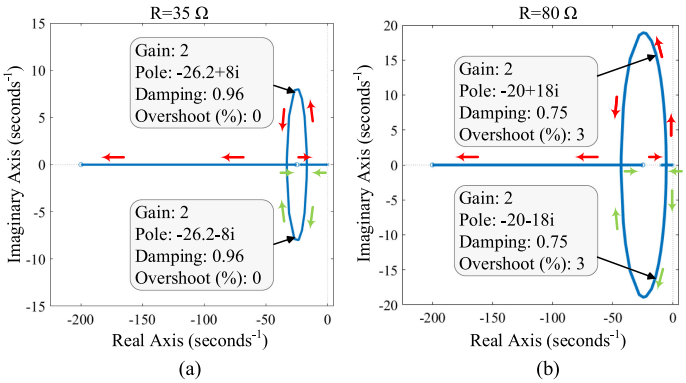

Fig. 12. Voltage control loop rlocus for (a) $R = 35\,\Omega$ and (b) $R = 80\,\Omega$.

which is obtained from the current control loop L_1 and presented in Fig. 11(a). To check the condition $d < 1$, the bode diagram of the duty cycle is plotted while considering the maximum value for the desired input in the current control loop ($I_{\rm max} = 30$ A in this article). If the magnitude of the bode diagram for all frequencies remains less than 0 dB, then the duty cycle is always less than 1. By considering all these conditions, $K_{\rm IH} = 1.5$ is selected to ensure the system's stability and achieve a settling time of less than 0.2 s. Fig. 11(b) shows the duty cycle d for $R = 35\,\Omega$ and $R = 80\,\Omega$ based on the selected parameters and confirms that d is less than 0 dB for all frequencies.

Step 2: To tune the voltage controller, we use the model presented in Fig. 6 and follow a similar procedure as the current controller design. The rlocus of the voltage control loop is shown in Fig. 12 for $R = 35\,\Omega$ and $R = 80\,\Omega$, while $K_{\rm PC}/K_{\rm IC} = 0.04$. Since the response of the outer voltage control loop must be slower than the inner current control loop, $K_{\rm IC} = 2$ is selected to achieve a settling time of less than 0.3 s.

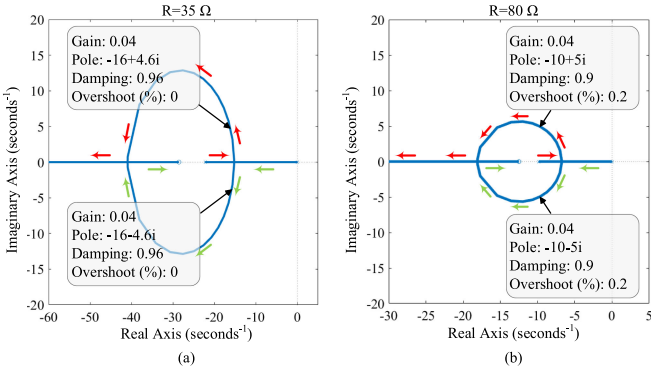

Fig. 13. Power control loop rlocus for (a) $R = 35\,\Omega$ and (b) $R = 80\,\Omega$.

TABLE III
COST COEFFICIENTS OF SOURCES

Source	α (¢)	β (¢/W)	γ (¢/W^2)
PV_1	90	1.2	1.0×10^{-4}
PV_2	85	1.19	1.5×10^{-4}
PV_3	95	1.2	0.5×10^{-4}
PV_4	80	1.21	1.25×10^{-4}

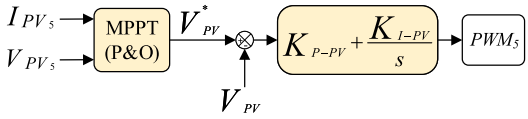

Fig. 14. MPPT control of PV_5.

Step 3: To tune the regulator and optimizer shown in Figs. 8 and 9, again, both the power regulating loop L_3 and the optimizing loops L_4 must be slower than L_1. In addition, L_3 and L_4 also need to be slower than the voltage control loop L_2 to allow it to work as the main controller. By setting $K_{\rm PR}/K_{\rm IR}$ and $K_{\rm PO}/K_{\rm IO}$ to 0.001 and using rloci for the power regulating loop with $R = 35\,\Omega$ and $R = 80\,\Omega$ (Fig. 13), the value 0.04 is selected for $K_{\rm IR}$. As a result, $K_{\rm IO}$ becomes $\frac{0.04}{2\gamma_{\rm mean}}$, where $\gamma_{\rm mean}$ is the mean value of all γ_i. Based on the cost coefficients presented in Table III, $\gamma_{\rm mean} = 0.0001$. Therefore, $K_{\rm IO} = 200$. It should be mentioned that the cost coefficients presented in Table III are set manually and are only for test analysis.

B. Design MPPT for PV_5

For PV_5, the reference voltage perturb and observe method [38] is used to transfer the maximum possible output power of the PV_5 to the dc bus (Fig. 14). In this case, the proportional gain ($K_{P-\rm PV}$) and the integral gain ($K_{I-\rm PV}$) of the controller are set to 0.0001 and 0.007, respectively.

C. Design the Controller for the BESS

To control the BESS, the voltage control loop designed in the proposed controller is used due to the similarity in the dynamic models of the boost converter and bidirectional converter.

V. RESULTS AND DISCUSSION

In this section, the proposed and different conventional control techniques are implemented on the DCMG shown in Fig. 1

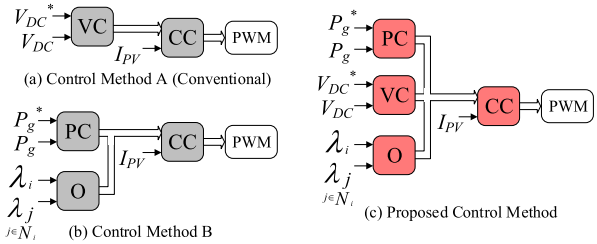

Fig. 15. Different control methods used for PV_1–PV_4.

using MATLAB/Simulink. The performance of the methods is compared through different case studies as follows: 1) during constant load demand; 2) during a step change of total generation power; 3) during a critical situation when one source of energy has failed; 4) during load demand variation; 5) during partial shading.

As already mentioned in Section IV, PV_5 is controlled by the MPPT algorithm presented in Fig. 14; and the powers transferred from the neighbor sources (PV_1–PV_4) are controlled by the proposed control algorithm with the connection presented by the adjacency matrix in

$$\mathbf{A} = \begin{array}{c} \\ \mathrm{PV}_1 \\ \mathrm{PV}_2 \\ \mathrm{PV}_3 \\ \mathrm{PV}_4 \end{array} \begin{array}{c} \begin{array}{cccc} \mathrm{PV}_1 & \mathrm{PV}_2 & \mathrm{PV}_3 & \mathrm{PV}_4 \end{array} \\ \begin{bmatrix} 0 & 1 & 0 & 1 \\ 1 & 0 & 1 & 0 \\ 0 & 1 & 0 & 1 \\ 1 & 0 & 1 & 0 \end{bmatrix} \end{array}. \tag{20}$$

The BESS is controlled by the conventional voltage controller shown in Fig. 6. In all the case studies, the dc-bus voltage profile, the total generation of all PVs and the charging/discharging performance of the BESS are shown and analyzed. The incremental costs (λ_1 to λ_4) of the neighbor sources (PV_1–PV_4) are calculated using (6), and the cost coefficients are presented in Table III.

A. Case Study 1: Control Methods Comparison

The objective of this case study is to compare the performance of the three control methods shown in Fig. 15. The three presented methods are differentiated based on their outer control loops: (a) Control method A is the conventional control method that is explained in Section II-D. It includes an outer voltage controller that generates a reference for the inner current controller. (b) Control method B includes an outer power controller and a cost optimizer connected in parallel. This method is considered as a basic solution for the optimization problem (1). (c) The proposed control method that combines the two other methods and is composed of three outer controllers: a voltage controller, a power controller, and the cost optimizer.

The dc bus is loaded with a total of 8.5-kW dc load; therefore, P_g^* is set to address the demanded power ($P_g^* = 8.5$ kW). The aim of all the control methods is to regulate the dc-bus voltage at 650 V while maintaining its variations within the standard limit ($\pm 6\%$ of nominal value) [39]. This is shown in Fig. 16(a), where all the three control methods successfully keep the dc-bus voltage within the standard $\pm 6\%$ limit. However, since control method B excludes the outer voltage controller, and the BESS of the DCMG is solely responsible for regulating the dc-bus voltage in this case, the dc-bus voltage exhibits higher fluctuations, 6.5%

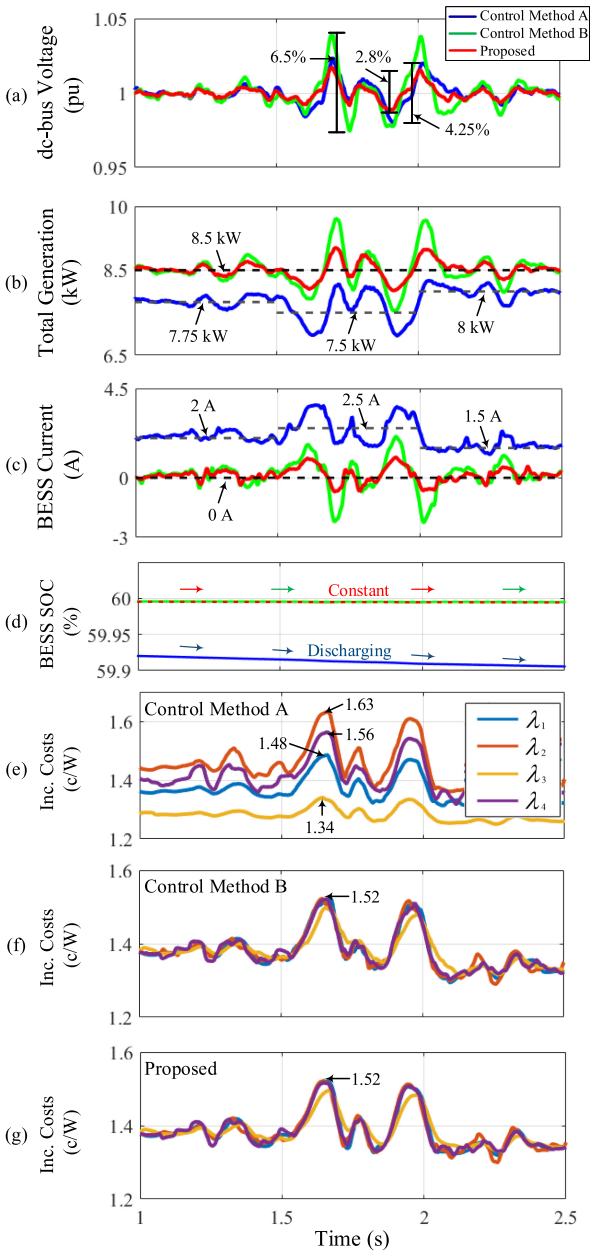

Fig. 16. Case study 1 in Section V-A. (a) DC-bus voltage. (b) Total generated power from PV_1 to PV_5. (c)–(d) BESS parameters. (e)–(g) Incremental costs.

(peak-to-peak) of the nominal voltage [Fig. 16(a)], as compared with the other two methods. By using the proposed controller, the fluctuations decrease to 2.8% because of receiving additional assistance from the outer voltage controller in regulating the dc-bus voltage. Using control method A, the fluctuations of the dc bus voltage are shown as 4.25% which is higher than the case when the proposed controller is used. As shown in Fig. 16(b), if control method B and the proposed controller are used, the total generation of all PVs is maintained at 8.5 kW which is equal to the load demand. Therefore, the output power of the BESS remains zero [Fig. 16(c)] and its SOC remains constant [Fig. 16(d)]. This can save the stored energy of the battery and, consequently, reduce the charging/discharging ratio of the battery increasing its lifetime. However, if control method A is used, the total generation changes between 7.5 and 8 kW, which is less than the load demand (8.5 kW). As a result, the BESS needs to discharge to support the DCMG. The positive output current of the BESS in Fig. 16(c) and the reduction of the battery's SOC in Fig. 16(d) demonstrate this operation.

The operation of the cost optimizer is shown in Fig. 16(f) and (g). As can be seen, the incremental costs of all neighbor sources are converged to an agreement, while these parameters are not controlled by control method A [Fig. 16(e)].

As a result of this case study, both control method B and the proposed controller exhibit significant savings in the stored energy of the battery and optimized cost compared with control method A. On the other hand, control method A and the proposed controller indicate lower fluctuations on the dc bus voltage in comparison to control method B. Therefore, this test shows that the proposed controller has the advantages of both control method A in maintaining the dc-bus voltage and control method B in saving the battery's energy as well as obtaining the constant power from all energy sources.

B. Case Study 2: Step Change of Total Generation Setpoint

The aim of this case study is to test the performance of the proposed controller upon a step change of total generation. In this test, the outputs of the proposed controller are compared in two different situations: 1) using a constant value for P_g^* and 2) changing the P_g^* during the test. It should be noted that control methods A and B are not considered for this test because of the inability of control method A to control the total generation and control method B to maintain a dc-bus voltage with less fluctuated.

In this test, the dc bus is loaded with a fixed 8.5-kW dc load. Between $t = 1$ s and $t = 1.5$ s, the proposed control system provides a constant total generated power for the DCMG via setting P_g^* at 8.5 kW as shown in Fig. 17(b). This maintains a balance between total generation and the loads' demand. As a result, the SOC of the BESS remains constant [Fig. 17(d)].

At $t = 1.5$ s, the P_g^* is adjusted at 12 kW to charge the BESS via generating excess power in the DCMG. As can be seen in Fig. 17(b), at $t = 1.5$ s, the total generated power increases from 8.5 to 12 kW following the reference signal. As a result, the dc-bus voltage experiences an overvoltage compared to the case in which $P_g^* = 8.5$ kW. As shown in Fig. 17(a), the overshoot is 3.5% with 0.2-s settling time, which is in the standard range ($\pm 6\%$ of nominal value) [39].

It should be noted that by increasing the total generation, the BESS starts charging to absorb the extra generated power via receiving –9 A current, as shown in Fig. 17(c), and the SOC of the battery starts increasing subsequently [Fig. 17(d)].

The other advantage of the proposed distributed coordinating control system is its ability to optimize cost as explained in detail in Section II-D. Such a superior performance is shown and validated in Fig. 17(e) and (f). As can be seen, by increasing P_g^* at $t = 1.5$ s, all the consensus values of PVs λ_i are converged to a new agreement that is higher than the consensus value when $P_g^* = 8.5$ kW [Fig. 17(f)].

Consequently, the results of this test confirmed the capability of the proposed distributed coordinating control in regulating the total output power generation, improving the BESS charging/discharging participation and cost minimization, which are not offered by conventional methods.

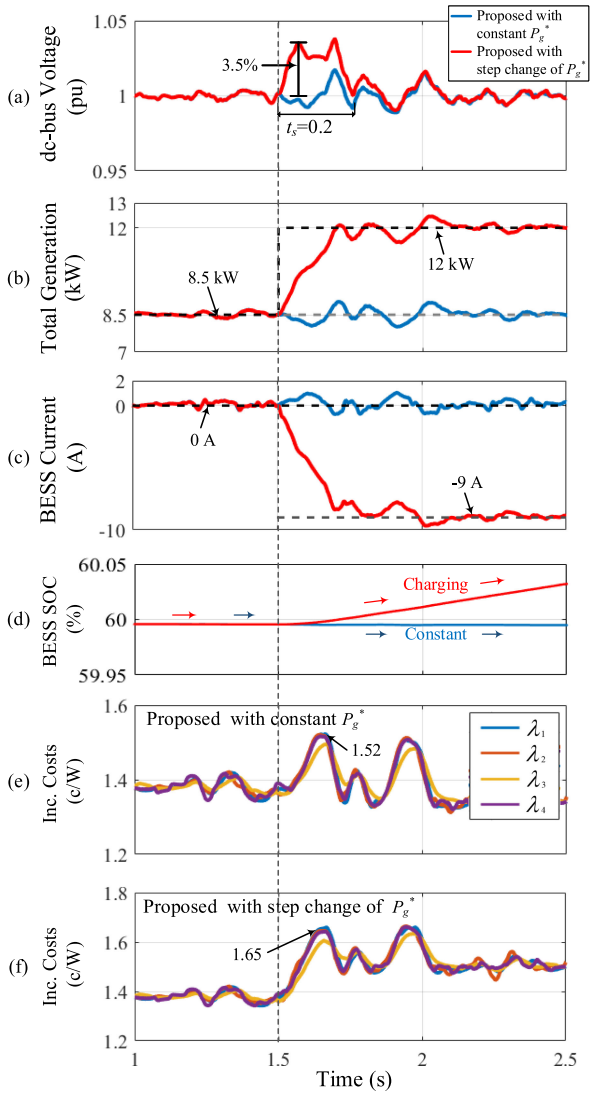

Fig. 17. Case study 2 in Section V-B. (a) DC-bus voltage. (b) Total generated power from PV_1 to PV_5. (c) and (d) BESS parameters. (e) and (f) Incremental costs.

C. Case Study 3: Power Source Failure

The aim of this test is to present the operation of the proposed distribution coordinating control system during a critical situation of a renewable energy source failure while the loads' demand is fixed at 8.5 kW. The results in Fig. 18 compare the performance of control method A with the proposed method with a power source failure. As the results show, if there is no power failure in the system, such as in the previous case studies, the proposed system exhibits superior performance compared with method A in terms of regulating the total generated power, improving BESS participation and minimizing costs.

At $t = 1.5$ s, the converter of PV_1 fails, and the protection system disconnects PV_1 from the DCMG as can be seen in Fig. 18(c). Thus, the total generation is reduced subsequently. To handle such a critical situation, the solution for control method A is to increase the discharged power of the BESS as shown in Fig. 18(d) and (e) to compensate for the lack of generation. This increases the stress on the battery and consumes its stored energy. However, using the proposed system, when PV_1 fails,

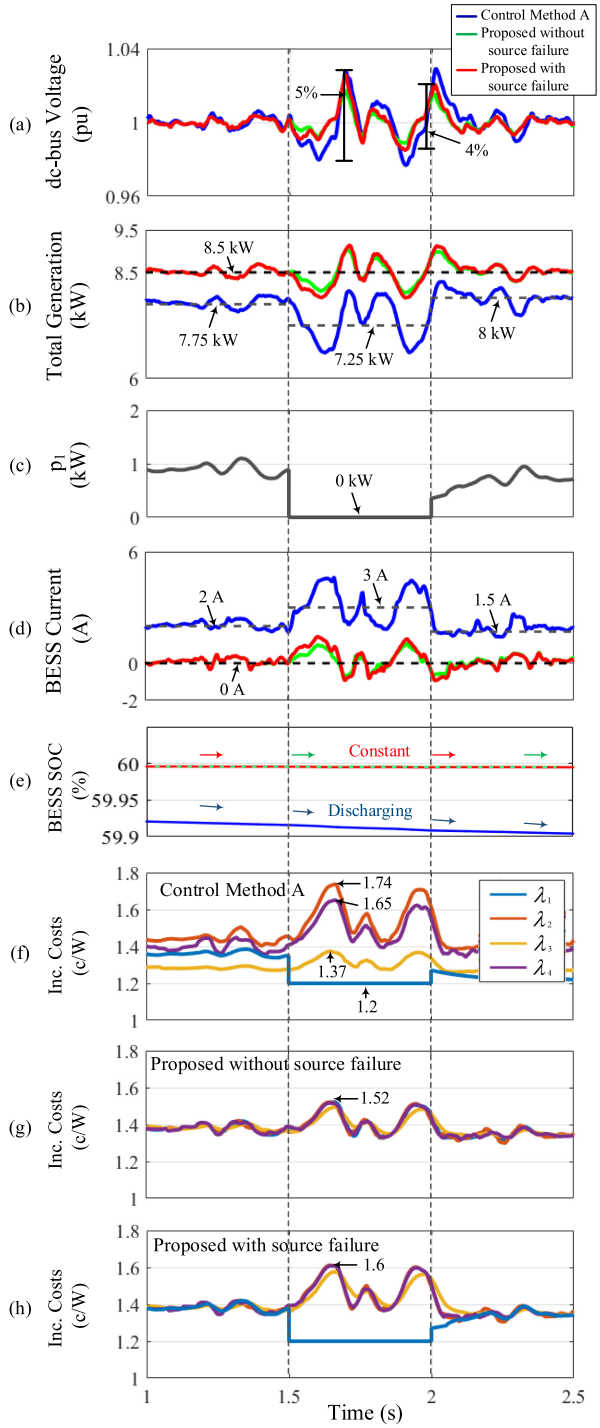

Fig. 18. Case study 3 in Section V-C. (a) DC-bus voltage. (b) Total generated power from PV_1 to PV_5. (c) Transferred power from PV_1. (d) and (e) BESS parameters. (f)–(h) Incremental costs.

the proposed power regulator immediately increases the output power of the other PVs to cover the lack of generation and reach the desired value P_g^* while regulating the dc-bus voltage V_{dc}. As a result, the stress on the BESS is significantly minimized while preserving its stored energy for the DCMG. The proposed controller also shows superior performance in minimizing the fluctuations of the dc-bus voltage compared with control method A [Fig. 18(a)]. Meanwhile, as can be seen in Fig. 18(h), the

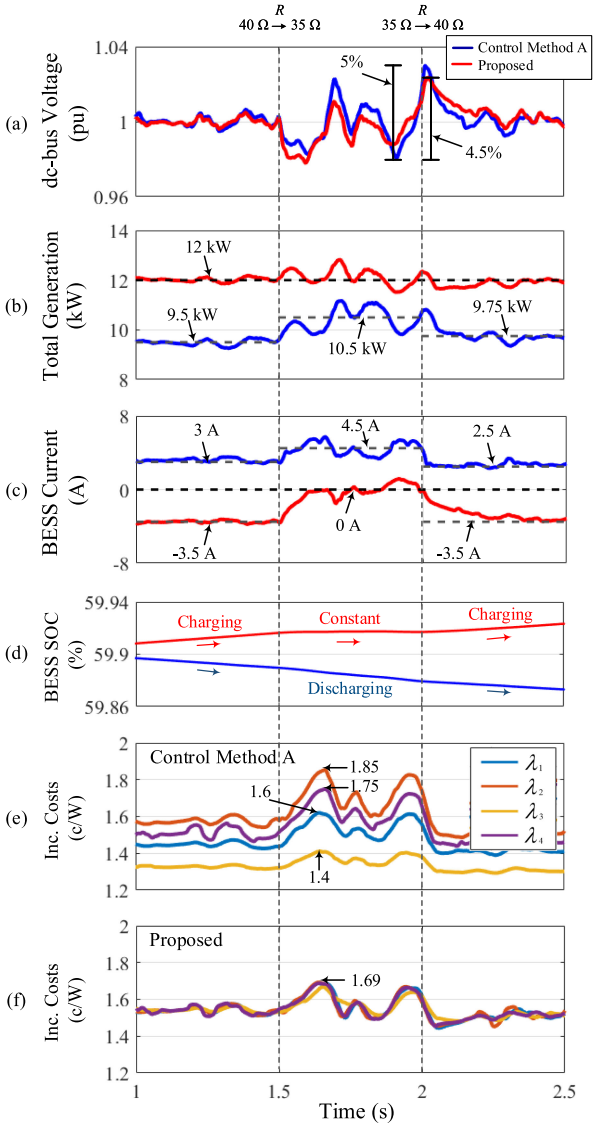

Fig. 19. Case study 4 in Section V-D. (a) DC-bus voltage. (b) Total generated power from PV_1 to PV_5. (c) and (d) BESS parameters. (e) and (f) Incremental costs.

costs are still perfectly minimized for the other operating PVs. The λ_1 for the failed PV_1 reaches its lowest value, and the other incremental costs converge to a higher consensus value [Fig. 18(h)]. At $t = 2$ s, the failed converter is fixed and plugged back into the system; thus, the proposed controller properly regulates the system to its normal operation.

D. Case Study 4: Load Variation

The objective of this case study is to analyze the performance of the proposed distributed coordinating controller in the DCMG under dc load variation. To do so, using the proposed system, P_g^* is kept constant at 12 kW; therefore, unlike the conventional system's performance, the total generated power of PVs remains constant throughout the test as shown in Fig. 19(b).

Between $t = 1$ s and $t = 1.5$ s, a 10-kW dc load is connected to the dc bus. While the proposed system regulates the total generated power at 12 kW, and this is more than the loads' demand, the proposed controller takes advantage of this mismatch and starts charging the BESS. This operation consumes the excess power and increases the SOC of the battery [Fig. 19(c) and (d)]. Using conventional method A, which does not have control over the PVs' output powers, the battery is in discharging mode to maintain the stability of the dc bus voltage.

Between $t = 1.5$ s and $t = 2$ s, the load is increased to 12 kW. During this time interval, the proposed control system shifts the BESS to standby mode since the generation and the loads' demand are equal. As a result, the SOC of the BESS becomes constant [Fig. 19(d)]. However, using control method A, the BESS is in discharging mode and its SOC is decreasing.

At $t = 2$ s, the dc loads' demand decreases from 12 to 10 kW, which can cause a voltage increase in the dc bus due to the lower load demand than generation. According to the performance of the conventional method, the BESS is in discharging mode. Nevertheless, as Fig. 19(b) shows, while the total generated power is still regulated at 12 kW using the proposed system, the battery is switched back to charging mode to improve its SOC [Fig. 19(d)]. As shown in Fig. 19(a), the proposed controller exhibits better performance in reducing the fluctuations of the dc-bus voltage compared with control method A.

The operation of the cost optimizer is shown in Fig. 19(f). As can be seen during the whole test, using the proposed control method, all the consensus values of PVs λ_i are converged to an agreement [Fig. 19(f)], while these parameters are not controlled by a conventional control approach [Fig. 19(e)].

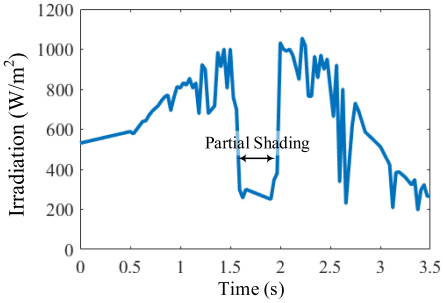

Fig. 20. Solar irradiation with partial shading applied to PV_5 in case study 5.

E. Case Study 5: Partial Shading

In this case study, the effect of partial shading is investigated on the dynamic of the DCMG. The solar irradiation pattern shown in Fig. 20 is applied to PV_5. As shown, partial shading occurs between $t = 1.5$ s and $t = 2$ s where the irradiation is significantly low (200 W/m^2), and, as a result, the output power of PV_5 is minimal during this time interval. During this test, the DCMG is loaded with a fixed 8.5-kW dc load, and P_g^* in the proposed controller is set at 8.5 kW. As shown in Fig. 21(a), the dc-bus voltage experiences less fluctuation when the proposed control method is used (2%) compared with the case when conventional control method A is used (3.8%). Fig. 21(b) validates that the operation of the proposed control approach in maintaining the total generation at a constant value (8.5 kW) despite the variable output power of PV_5 [Fig. 21(c)] due to the presence of partial shading in its input irradiance between $t = 1.5$ s and $t = 2$ s. By using control method A, the total generation in Fig. 21(b) decreases during partial shading, and the BESS has to inject more power to compensate for the

TABLE IV
COMPARISON OF THE PROPOSED AND THE CONVENTIONAL CONTROL METHOD

Test		V_{DC} fluctuation	Total generation	BESS		Incremental costs			
		$V_{DC(p-p)}$ (%)	P_g (kW)	I_{BESS} (A)	SOC	λ_1 (c/W)	λ_2 (c/W)	λ_3 (c/W)	λ_4 (c/W)
Constant load	Conventional	4.25	7.5 to 8	1.5 to 2.5	*decreasing*	1.48	1.63	1.34	1.56
	Proposed	2.8	8.5	0	*constant*	1.52	1.52	1.52	1.52
Load variation	Conventional	5	9.5 to 10.5	2.5 to 4.5	*decreasing*	1.6	1.85	1.4	1.75
	Proposed	4.5	12	-3.5 to 0	*increasing*	1.69	1.69	1.69	1.69
Power source failure	Conventional	5	7.25 to 8	1.5 to 3	*decreasing*	1.2	1.74	1.37	1.65
	Proposed	4	8.5	0	*constant*	1.2	1.6	1.6	1.6
Partial shading	Conventional	3.8	7 to 8	1.5 to 3.5	*decreasing*	1.48	1.62	1.34	1.56
	Proposed	2	8.5	0	*constant*	1.52	1.52	1.52	1.52
Conclusion	Conventional	*High*	*uncontrollable*	*discharging*		*divergent*			
	Proposed	*Low*	*controllable*	*constant/charging*		*convergent*			

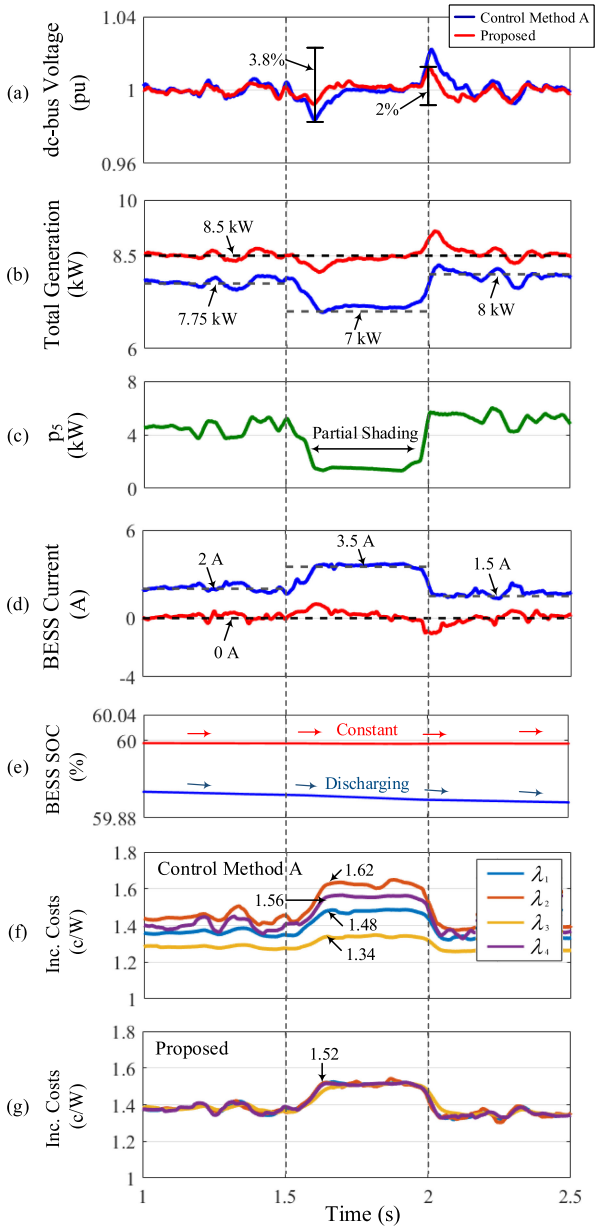

Fig. 21. Case study 5 in Section V-E. (a) DC-bus voltage. (b) Total generated power from PV_1 to PV_5. (c) Output power of PV_5. (d) and (e) BESS parameters. (f) and (g) Incremental costs.

power shortage [Fig. 21(d)]. Fig. 21(f) and (g) shows that the incremental costs of all neighbor sources inevitably increase during the partial shading, which is caused by the need to receive more power from the neighbor sources (PV_1–PV_4). However, if the proposed control method is used, the cost for this extra power is less since all the incremental costs are converged to an agreement [Fig. 21(g)] compared with the conventional method, which has no control over the incremental costs [Fig. 21(f)].

Table IV briefly summarizes the performance of the proposed controller in comparison to the performance of the conventional control method. Using the proposed controller, the total generation is adjustable irrespective of changes in PV outputs, while the total generation is nonconstant and uncontrollable by using the conventional control method. In addition, the charging/discharging ratio of the BESS is decreased by using the proposed controller. By using the proposed controller, the cost is minimized via forcing the incremental costs of all sources to converge to an agreement, while by using the conventional controller, the cost issue is not considered and the incremental costs are different.

VI. CONCLUSION

An optimized distributed coordinating control system is proposed for a multi-PV energy source in an islanded DCMG. The presented method improves the performance of the conventional primary control by having a dc-bus voltage regulator, a power regulator, and an energy cost optimizer. Five case studies in a real-time simulation platform analyzed the performance of the proposed method during both normal operations and critical situations of renewable energy failure in the DCMG. The results validate that the power regulator can successfully adjust the total generated power of all PVs to receive a constant value for the total generated power in the DCMG. Moreover, the charging/discharging fluctuations of the BESS are significantly reduced, and more energy is stored in the BESS to support the DCMG during the absence of sunlight or when the PVs are in standby mode. Furthermore, the energy cost optimizer in the proposed control method minimizes the total generation cost using the consensus algorithm. The results validate that the proposed distributed control method can be a reliable and effective alternative for a multi-PV islanded DCMG. A future extension of this article would be to experimentally implement the proposed control method in a real islanded DCMG.

REFERENCES

[1] F. He, Z. Zhao, L. Yuan, and S. Lu, "A DC-link voltage control scheme for single-phase grid-connected PV inverters," in *Proc. IEEE Energy Convers. Congr. Expo.*, 2011, pp. 3941–3945.

[2] M. S. Rahman, M. Hossain, J. Lu, and H. R. Pota, "A need-based distributed coordination strategy for EV storages in a commercial hybrid AC/DC microgrid with an improved interlinking converter control topology," *IEEE Trans. Energy Convers.*, vol. 33, no. 3, pp. 1372–1383, Sep. 2018.

[3] V. N. Lal and S. N. Singh, "Control and performance analysis of a single-stage utility-scale grid-connected PV system," *IEEE Syst. J.*, vol. 11, no. 3, pp. 1601–1611, Sep. 2017.

[4] X. Liu, P. Wang, and P. C. Loh, "A hybrid AC/DC microgrid and its coordination control," *IEEE Trans. Smart Grid*, vol. 2, no. 2, pp. 278–286, Jun. 2011.

[5] R. Singh, S. Taghizadeh, N. M. L. Tan, and J. Pasupuleti, "Battery energy storage system for pv output power leveling," *Adv. Power Electron.*, vol. 2014, pp. 1–11, 2014.

[6] D. V. De La Fuente, C. L. T. Rodríguez, G. Garcerá, E. Figueres, and R. O. Gonzalez, "Photovoltaic power system with battery backup with grid-connection and islanded operation capabilities," *IEEE Trans. Ind. Electron.*, vol. 60, no. 4, pp. 1571–1581, Apr. 2013.

[7] R. Singh, S. Taghizadeh, N. M. Tan, and S. Mekhilef, "Experimental verification of a battery energy storage system for integration with photovoltaic generators," *Adv. Power Electron.*, vol. 2017, pp. 1–10, 2017.

[8] S. Moayedi and A. Davoudi, "Unifying distributed dynamic optimization and control of islanded DC microgrids," *IEEE Trans. Power Electron.*, vol. 32, no. 3, pp. 2329–2346, Mar. 2017.

[9] V. Nasirian, A. Davoudi, F. L. Lewis, and J. M. Guerrero, "Distributed adaptive droop control for DC distribution systems," *IEEE Trans. Energy Convers.*, vol. 29, no. 4, pp. 944–956, Dec. 2014.

[10] Q. Shafiee, T. Dragičević, J. C. Vasquez, and J. M. Guerrero, "Hierarchical control for multiple DC-microgrids clusters," *IEEE Trans. Energy Convers.*, vol. 29, no. 4, pp. 922–933, Dec. 2014.

[11] M. Kumar, S. Srivastava, and S. Singh, "Control strategies of a DC microgrid for grid connected and islanded operations," *IEEE Trans. Smart Grid*, vol. 6, no. 4, pp. 1588–1601, Jul. 2015.

[12] K. Sun, L. Zhang, Y. Xing, and J. M. Guerrero, "A distributed control strategy based on DC bus signaling for modular photovoltaic generation systems with battery energy storage," *IEEE Trans. Power Electron.*, vol. 26, no. 10, pp. 3032–3045, Oct. 2011.

[13] N. L. Diaz, T. Dragičević, J. C. Vasquez, and J. M. Guerrero, "Intelligent distributed generation and storage units for DC microgrids-a new concept on cooperative control without communications beyond droop control," *IEEE Trans. Smart Grid*, vol. 5, no. 5, pp. 2476–2485, Sep. 2014.

[14] N. Poursafar, S. Taghizadeh, and M. Hossain, "An optimized power management system for an islanded DC microgrid," in *Proc. 29th Australais. Univ. Power Eng. Conf.*, 2019, pp. 1–6.

[15] P. Mathew, S. Madichetty, and S. Mishra, "A multilevel distributed hybrid control scheme for islanded DC microgrids," *IEEE Syst. J.*, vol. 13, no. 4, pp. 4200–4207, Dec. 2019.

[16] S. K. Sarkar, M. H. K. Roni, D. Datta, S. K. Das, and H. R. Pota, "Improved design of high-performance controller for voltage control of islanded microgrid," *IEEE Syst. J.*, vol. 13, no. 2, pp. 1786–1795, Jun. 2019.

[17] Y. Xia, M. Yu, P. Yang, Y. Peng, and W. Wei, "Generation-storage coordination for islanded dc microgrids dominated by PV generators," *IEEE Trans. Energy Convers.*, vol. 34, no. 1, pp. 130–138, Mar. 2019.

[18] B. Babaiahgari, M. H. Ullah, and J.-D. Park, "Coordinated control and dynamic optimization in dc microgrid systems," *Int. J. Elect. Power Energy Syst.*, vol. 113, pp. 832–841, 2019.

[19] J. Li, Q. Yang, F. Robinson, F. Liang, M. Zhang, and W. Yuan, "Design and test of a new droop control algorithm for a SMES/battery hybrid energy storage system," *Energy*, vol. 118, pp. 1110–1122, 2017.

[20] Y. Pu, Q. Li, W. Chen, and H. Liu, "Hierarchical energy management control for islanding dc microgrid with electric-hydrogen hybrid storage system," *Int. J. Hydrogen Energy*, vol. 44, no. 11, pp. 5153–5161, 2019.

[21] P. Prabhakaran, Y. Goyal, and V. Agarwal, "Novel nonlinear droop control techniques to overcome the load sharing and voltage regulation issues in DC microgrid," *IEEE Trans. Power Electron.*, vol. 33, no. 5, pp. 4477–4487, May 2018.

[22] S. Sahoo, S. Mishra, S. Jha, and B. Singh, "A cooperative adaptive droop based energy management and optimal voltage regulation scheme for DC microgrids," *IEEE Trans. Ind. Electron.*, vol. 67, no. 4, pp. 2894–2904, Apr. 2020.

[23] Y. Shan, J. Hu, M. Liu, J. Zhu, and J. M. Guerrero, "Model predictive voltage and power control of islanded PV-battery microgrids with washout-filter-based power sharing strategy," *IEEE Trans. Power Electron.*, vol. 35, no. 2, pp. 1227–1238, Feb. 2020.

[24] S. Batiyah, N. Zohrabi, S. Abdelwahed, and R. Sharma, "An MPC-based power management of a PV/battery system in an islanded DC microgrid," in *Proc. IEEE Transp. Electrific. Conf. Expo.*, 2018, pp. 231–236.

[25] T. Dragičević, J. M. Guerrero, J. C. Vasquez, and D. Škrlec, "Supervisory control of an adaptive-droop regulated dc microgrid with battery management capability," *IEEE Trans. Power Electron.*, vol. 29, no. 2, pp. 695–706, Feb. 2014.

[26] V. Dash and P. Bajpai, "Power management control strategy for a stand-alone solar photovoltaic-fuel cell-battery hybrid system," *Sustain. Energy Technol. Assessments*, vol. 9, pp. 68–80, 2015.

[27] R. A. Biroon, Z. Abdollahi, and R. Hadidi, "Inverter's nonlinear efficiency and demand-side management challenges," *IEEE Power Electron. Mag.*, vol. 8, no. 1, pp. 49–54, Mar. 2021.

[28] S. Kotra and M. K. Mishra, "Design and stability analysis of DC microgrid with hybrid energy storage system," *IEEE Trans. Sustain. Energy*, vol. 10, no. 3, pp. 1603–1612, Jul. 2019.

[29] B. R. Ravada and N. R. Tummuru, "Control of a supercapacitor/battery/PV based stand-alone dc-microgrid," *IEEE Trans. Energy Convers.*, vol. 35, no. 3, pp. 1268–1277, Sep. 2020.

[30] A. A. K. Arani, G. B. Gharehpetian, and M. Abedi, "A novel control method based on droop for cooperation of flywheel and battery energy storage systems in islanded microgrids," *IEEE Syst. J.*, vol. 14, no. 1, pp. 1080–1087, Mar. 2020.

[31] L. Shen, Q. Cheng, Y. Cheng, L. Wei, and Y. Wang, "Hierarchical control of dc micro-grid for photovoltaic EV charging station based on flywheel and battery energy storage system," *Electric Power Syst. Res.*, vol. 179, 2020, Art. no. 106079.

[32] R. Chenni, M. Makhlouf, T. Kerbache, and A. Bouzid, "A detailed modeling method for photovoltaic cells," *Energy*, vol. 32, no. 9, pp. 1724–1730, 2007.

[33] A. J. Wood, B. F. Wollenberg, and G. B. Sheblé, *Power Generation, Operation, and Control*. Hoboken, NJ, USA: Wiley, 2013.

[34] Z. Wang, W. Wu, and B. Zhang, "A distributed control method with minimum generation cost for DC microgrids," *IEEE Trans. Energy Convers.*, vol. 31, no. 4, pp. 1462–1470, Dec. 2016.

[35] H. Han, H. Wang, Y. Sun, J. Yang, and Z. Liu, "Distributed control scheme on cost optimisation under communication delays for DC microgrids," *IET Generation, Transmiss. Distrib.*, vol. 11, no. 17, pp. 4193–4201, 2017.

[36] W. Ren and R. W. Beard, *Distributed Consensus in Multi-Vehicle Cooperative Control*. Berlin, Germany: Springer, 2008.

[37] R. W. Erickson and D. Maksimovic, *Fundamentals of Power Electronics*. Berlin, Germany: Springer Science & Business Media, 2007.

[38] M. A. Elgendy, B. Zahawi, and D. J. Atkinson, "Assessment of perturb and observe MPPT algorithm implementation techniques for PV pumping applications," *IEEE Trans. Sustain. Energy*, vol. 3, no. 1, pp. 21–33, Jan. 2012.

[39] B. Noone, *PV Integration on Australian Distribution Networks: Literature Review*. Kensington, Australia: The Australian PV Assoc., UNSW, 2013.